Journal of Network Intelligence
Taiwan Ubiquitous Information
 ISSN 2414-8105 (Online)
Volume **9**, Number **2**, May **2024**

Dehazing Quality Evaluation Algorithm Integrating Dark Channel Theory and Image Depth Estimation

Jia-Yan Huang, Xin-Xin Xu, Shao-Ye Luo
New Engineering Industry College
Putian University, Putian 351100, China
jyan_huang@163.com, XxinXu04@163.com, lsy123@163.com

Wan-Qi Zhao
The University of Sheffield, Sheffield S10 2TN, United Kingdom
wanqizhao0110@163.com

Hao-Yi Fan
School of Computer and Artificial Intelligence
Zhengzhou University, Zhengzhou 450001, China
fanhaoyi@zzu.edu.cn

Antoni Grau, Edmundo Guerra, Chuan-Sheng Wang*
Department of Automatic Control Technical
Polytechnic University of Catalonia, Barcelona 08034, Spain
antoni.grau@upc.edu, edmundo.guerra@upc.edu, wangcleaner@gmail.com

Fu-Quan Zhang*
Fujian Provincial Key Laboratory of Information Processing and Intelligent Control
Minjiang University, Fuzhou 350108, China
zfq@mju.edu.cn

*Corresponding author: Chuan-Sheng Wang and Fu-Quan Zhang

Received August 23, 2023, revised November 9, 2023, accepted February 19, 2024.

Abstract. Image dehazing is an important research topic and hotspot in the fields of image processing and computer vision. Therefore, evaluating the performance of image dehazing algorithms has become an import research issue. However, current image quality assessment (IQA) algorithms only judge the final dehazed image and do not give an analysis of the capabilities of the image dehazing algorithm. In order to fill this gap, we propose an image dehazing quality assessment method that integrated the dark channel prior with image depth estimation. The proposed method first uses the dark channel prior to estimate the absolute amount of haze removed from each pixel as an indication of the performance of dehazing. Then, a dual-scale variance ratio method is introduced to estimate the scene depth of the image. Finally, the relative dehazing is calculated from the obtained absolute dehazing and the image depth to represent the capability of the dehazing algorithm. The method proposed in this paper first introduces the concepts of relative and absolute dehazing quantities, along with pioneering a pixel-level evaluation of dehazing outcomes. Extensive experiments show that the algorithm proposed in this paper is more in line with human subjective judgment than other IQA algorithms.

Keywords: image dehazing, dehazing evaluation, depth estimation, dark channel prior, pixel-level estimation.

1. **Introduction.** Image dehazing is an important research topic and a current hotspot in the fields of image processing and computer vision [1]. In various practical applications such as traffic monitoring and security inspection systems, the majority require high-definition images as input [2, 3, 4]. However, if these uncorrected images are fed into an outdoor surveillance system, there is a great likelihood that the results of the system's normal operation will be affected, leading to the occurrence of significant errors. This disruption could potentially lead to critical errors with substantial implications. As a result, image dehazing has attracted increasing attention from a growing number of researchers.

Haze and fog can lead to a decrease in image quality, significantly impacting the visual quality and post-processing of images. Due to the practicality of image dehazing, many researchers have conducted studies in this area [5, 6]. Furthermore, there are various methods for evaluating image quality [7, 8, 9, 10, 11, 12]. However, there has been very little dedicated research on objective evaluation methods specifically for dehazing. If the dehazing results can be accurately assessed, it would be possible to choose the most suitable dehazing algorithm for different scenes. Unfortunately, when assessing the effectiveness of dehazing algorithms, the existing methods primarily rely on subjective visual evaluations. Subjective evaluations are susceptible to personal biases, leading to less reliable evaluation outcomes. Consequently, it is evident that achieving an objective and quantitative assessment of dehazing effects remains a challenge yet to be effectively addressed.

Existing objective IQA methods can be classified into three categories based on their requirement for reference information: full-reference, reduced-reference, and no-reference methods, with the first two categories relying on reference images. Concerning the specific application of evaluating image dehazing effects, the existing objective evaluation methods can be broadly categorized into two types. The first type measures the dehazing performance solely from the perspective of image contrast. For instance, the Contrast Enhancement Assessment method [13], proposed by Hautiere et al., indirectly assesses dehazing algorithms by obtaining a contrast map through visible edge detection. However, this method fails to accurately evaluate images with excessive enhancement. The reduced-reference based methods consider both image contrast and color in a comprehensive manner. For example, global and local contrast metrics are employed by Wang et al. to gauge the degree of contrast enhancement in dehazed images. Additionally, evaluation metrics such as hue polar histogram, principal component analysis of RGB image, and histogram similarity are used to assess color quality from the perspectives of color restoration ability, color rendition ability, and natural color representation. Li et al. used Canny operator and bright channel to detect the effective edge intensity of the dehazed image, while histogram similarity was used in color evaluation to measure the color reproduction ability of the dehazed image [14]. Zhang et al. proposed the evaluation indexes of reduction coefficient and color reduction coefficient, which are also aimed at the contrast and color of the image to objectively evaluate the dehazing performance.

All current algorithms for evaluating the effectiveness of dehazing have roughly the following three drawbacks:

1. Many algorithms are not specialized in objective evaluation methods for dehazing quality, so these algorithms are not able to objectively evaluate the quality of image dehazing, which results in these methods not having good reliability.
2. When these algorithms are utilized to do image dehazing evaluation, they also can only get the evaluation of the whole image, and cannot be accurate to the evaluation of a specific pixel point.

3. It is well known that since under normal circumstances, the further away the scene is from the camera, then the more severely the obtained image is affected by haze, so the third flaw of the above algorithms is that the evaluation of the image dehazing performance is not combined with the depth of the image.

In this paper, an effective method for evaluating the effect of image dehazing is proposed by combining the dark channel prior theory. The algorithm proposed in this paper has the following three advantages:

1. This algorithm is specifically designed to evaluate the dehazing performance of the image and therefore has some reliability.
2. This algorithm not only evaluates the whole image but also evaluates each pixel point.
3. This algorithm considers the relationship between scene depth and haze amount when evaluating the quality of dehazing, which has not been considered in all previous algorithms.

Experiment results show that compared with several existing classical methods for evaluating the effect of dehazing, the method proposed in this paper is not only more consistent with human subjective judgment, but also more objective.

2. **Related Work.**

In this section, we review the relevant work on IQA. Evaluating image quality is a highly challenging task due to the distinct characteristics of different types of image distortions. Moreover, the diversity of image content introduces further challenges to IQA. IQA can be broadly categorized into two types: traditional models based on prior knowledge and models based on convolutional neural networks.

2.1. **Traditional image quality assessment.**

In traditional Image Quality Assessment (IQA) algorithms, features are extracted based on the characteristics of image distortions. Natural scene statistics serve as a common example of this approach. Methods such as Directionally Individuated Visual Estimation (DIVINE) using oriented pyramids [15] and Blind Image Integrity Notator using DCT coefficients (BLIINDS) [16] fall under the umbrella of natural scene statistics. While traditional models perform well when evaluating images with synthetic distortions, their capabilities are often constrained when predicting image quality in real-world scenarios.

2.2. **Learning-based image quality assessment.**

Due to the immense success of deep learning in computer vision tasks [1, 17], many researchers have turned their attention to IQA models based on convolutional neural networks (CNNs). CNNs can extract reliable semantic features from deep architectures and then be fine-tuned for prediction with appropriate modifications. Given the lack of large-scale data directly related to image quality, most CNN-based models employ transfer learning techniques, using pretrained models (typically pretrained on ImageNet [18]) and fine-tuning them with actual image quality labels.

Zhang et al. [19] employed two separate CNNs to handle real scenes and artificially synthesized scenes independently. Kim et al. [20] used Full-Reference IQA (FR-IQA) as an intermediate regression target during training. Zeng et al. [21] utilized statistical distribution of subjective scores during training, leading to faster convergence and superior quality estimation. Su et al. [22] introduced an adaptive hyper-network architecture to decouple quality prediction from content understanding. Ying et al. [23] demonstrated that training with both image and patch quality scores significantly improved model performance. These authors' developed PaQ-2-PiQ algorithm also benefited from the availability of an exceptionally large real distortion image subjective database. All these models rely on

specific supervised fine-tuning mechanisms to achieve enhanced performance. In contrast, our work focuses on unsupervised feature learning, eliminating the need for fine-tuning processes. This distinction sets our approach apart from the aforementioned methods.

3. **Methods.** This paper proposes an image dehazing quality assessment algorithm based on the dark channel prior and image depth estimation. The algorithmic workflow of this paper is illustrated in Figure 1. Its main steps encompass pixel-level absolute dehazing estimation, image depth estimation, and pixel-level relative dehazing estimation. Compared to traditional image dehazing evaluation methods, the algorithm presented in this paper introduces a pixel-level image dehazing evaluation. This enables the assessment of the dehazing effect at each individual pixel in an image. This approach not only serves for evaluating the dehazing effect of an image but also guides further dehazing processing for localized image regions with suboptimal dehazing results. Firstly, the depth information of the image is computed. Subsequently, the dehazing amount for specific pixels in the experimental image is calculated. Finally, the dehazing amount for each pixel is divided by its corresponding depth value. This yields a quantified value representing the dehazing capability of the current dehazing algorithm at the given pixel location. By calculating the average of these values, the overall dehazing effectiveness evaluation for the entire image is obtained.

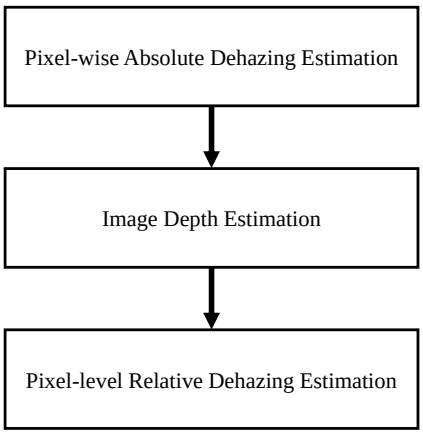

FIGURE 1. Flowchart of the proposed method in this paper.

3.1. **Dark channel prior.** He et al. [6] proposed a dark channel prior knowledge for image dehazing. This prior knowledge is obtained through statistical analysis of a large number of outdoor haze-free images, suggesting that the majority of pixels in haze-free outdoor images, except in the sky region, have very low values in at least one of the RGB color channels.

For any given image I, its dark channel can be defined as follows:

$$I^{dark}(i,j) = \min_{(k,l)\in\Omega(i,j)} (\min_{c\in(r,g,b)} I^c(k,l)) \tag{1}$$

In this equation, I_c represents a color channel of I, and $\Omega(i,j)$ is a local neighborhood region contered at pixel (i,j). Extensive experiments in [6] have demonstrated the effectiveness of the dark channel prior in the image dehazing process.

3.2. **Depth estimation.** How to extract the structure and attributes of the three-dimensional world from two-dimensional images is a fundamental problem in computer vision [24, 25]. Therefore, automatically extracting image depth information from one or multiple images, namely performing depth estimation, is a significant research area in computer vision.

Currently, mainstream methods for scene depth estimation can be divided into two categories: active vision (AV) approaches and passive vision (PV) approaches. Active vision methods involve emitting controlled beams of light towards the object of interest, then capturing the images formed by these beams on the object's surface. The distance to the object is calculated through geometric relationships to estimate scene depth. Passive vision methods, on the other hand, usually do not employ special light sources for illumination. They estimate scene depth solely from one or multiple two-dimensional image information obtained from one or more camera systems.

This paper studies and proposes a single-image depth estimation algorithm based on the ratio of dual-scale local neighborhood variances. This algorithm falls under the category of passive vision methods. The method utilizes the minimum-to-maximum ratio of pixel-wise local neighborhood window grayscale variances at two different scales to estimate image depth. The principle behind this lies in the fact that images of natural scenes often exhibit variations due to the varying distances between objects and the camera during the capture process. Distant parts of the scene tend to be less sharp with fewer details, resulting in similar grayscale variances for local neighborhood windows at both scales, yielding a ratio close to 1. Conversely, closer objects in the scene tend to have sharper images with more details, leading to significant differences in grayscale variances between local neighborhood windows at two scales, resulting in a ratio far from 1. Furthermore, compared to regular natural images, hazy images are better suited for estimating image depth using the ratio of minimum-to-maximum grayscale variances of pixel-wise local neighborhood windows at two scales. This is because in hazy images, distant regions are often characterized by a higher concentration of haze particles suspended in the air, which further blurs the details of the distant areas. As a result, the ratio of grayscale variances for local neighborhood windows at both scales tends to be closer to 1 for these regions. In contrast, areas with less haze in closer regions have less impact on image details, causing the ratio of minimum-to-maximum grayscale variances of pixel-wise local neighborhood windows to remain distant from 1. Therefore, the dual-scale local neighborhood variance ratio can be used to estimate the image depth information at each pixel. For a given pixel $p(i, j)$ and two different scales S and L, the image depth estimation process at this pixel is illustrated in Figure 2:

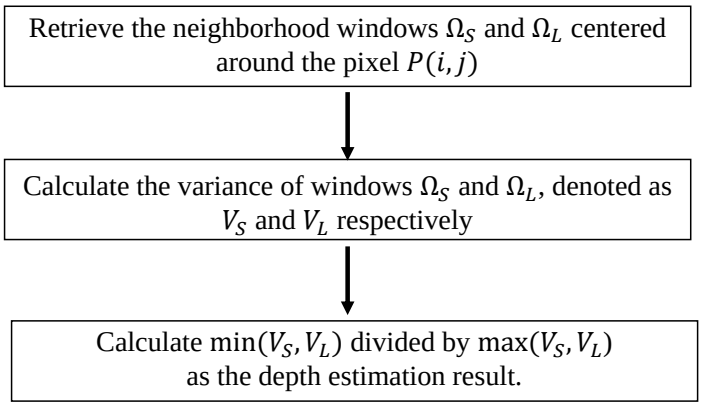

FIGURE 2. Depth Estimation Process.

To validate the effectiveness of the proposed method for image depth estimation, the image shown in Figure 1(a) is taken as an example, and Figure 2 presents its depth estimation results.

3.3. **Absolute Dehazing Amount.** The dark channel prior theory [6] introduces the concept of the dark channel. Inspired by this, this paper proposes a minimum channel concept. For any given image I, its minimum channel is defined as follows:

$$I^{min}(i,j) = \min_{c\in(r,g,b)} I^c(i,j) \tag{2}$$

here, (i,j) represents a pixel point, and $\min_{c\in(r,g,b)}$ indicates selecting the minimum brightness value from the RGB three channels.

The dark channel prior theory [6, 26, 27] suggests that for outdoor haze-free images, the dark channel values of most pixels outside the sky region are close to 0. Therefore, the difference between the minimum channel value of a hazy image and the minimum channel value of its dehazed result can be used to quantify the absolute dehazing amount of an image. Its formal description is as follows:

$$H(i,j) = I^{min}(i,j) - J^{min}(i,j) \tag{3}$$

here, $H(i,j)$ represents the absolute dehazing amount at pixel (i,j), and $I^{\min}(i,j)$ and $J^{\min}(i,j)$ respectively denote the minimum channel values of the hazy original image and the dehazed result image."

Figure 3(a)-(d) shows the original hazy image of a natural scene, the dehazed image, the minimum channel image of the hazy input and the minimum channel image of the dehazed result, respectively.

(a) Original hazy image (b) Dehazed image

(c) Minimum channels for hazed images (d) Minimum channels for fog-free images

FIGURE 3. Minimum channel map of the hazy image and the dehazed image.

3.4. **Relative Dehazing Amount.** The absolute dehazing amount can only characterize the extent of dehazing at a specific pixel, but it cannot fully capture the quality of the dehazing effect. This is because different image regions at varying scene depths have different amounts of haze content. Distant regions often have more haze content than closer ones. The dehazing effect brought about by the same absolute dehazing amount in distant and close regions can differ. To address this, this paper combines image depth

estimation and introduces a concept of relative dehazing amount to describe the dehazing effect at a particular pixel using an algorithm. The definition of relative dehazing amount is as follows:

$$\widetilde{H}(i,j) = H(i,j)/D(i,j) \tag{4}$$

here, $H(i,j)$ represents the absolute dehazing amount at pixel (i,j), $D(i,j)$ represents the dehazing capability of the algorithm at that point, and (10) denotes the scene depth estimation value at pixel (i,j).

For the entire hazy image, the dehazing effectiveness of the algorithm is defined as follows:

$$\widetilde{H}(x) = \frac{1}{MN}\sum_{i=1}^{M}\sum_{j=1}^{N}\widetilde{H}(i,j) \tag{5}$$

where M and N represent the number of rows and columns of the image, respectively.

4. **Experiments.** In order to validate the efficacy of the algorithm proposed in this paper, we conducted grouping experiments using diverse sets of images. The representative image dehazing algorithms chosen for the experiments include: DCP [6], Histogram Equalization and Tarel et al. [28]. The rationale behind selecting these algorithms is as follows: Global histogram equalization is one of the most commonly employed image enhancement techniques, renowned for its exceptional contrast enhancement capabilities. The algorithms by He et al. and Tarel et al. are recognized for their simplicity and effectiveness, with DCP, in particular, emerging as a focal point of research in the field of image dehazing in recent years. In addition, to validate the effectiveness and robustness of the proposed IQA method, we conducted an analysis of its performance on a self-constructed dataset. This database encompasses a diverse range of data, facilitating a comprehensive assessment of the method's performance. An example of the data used in this study is illustrated in Figure 4. The image database at our disposal comprises a total of sixty images, encompassing diverse scenes including aerial landscapes, architectural structures, forest vistas, cityscapes, indoor gardens, as well as beaches.

FIGURE 4. Example images of the dataset.

4.1. **Image quality evaluation algorithms.** Considering the absence of a standardized criterion for objective IQA within the realm of image dehazing, this section will initially employ several commonly utilized objective evaluation metrics associated with digital image processing. The metrics selected for this study include Peak Signal-to-Noise Ratio (PSNR), Mean Gradient, and Color Image Information Entropy.

The Peak Signal-to-Noise Ratio (PSNR), commonly established through the utilization of Mean Square Error (MSE), serves as a prevalent metric. In the context of two monochromatic images, denoted as l and k, each characterized by dimensions of $m \times n$, if one image can be reasonably approximated by the other with the inclusion of noise, their respective Mean Square Error is articulated as follows:

$$MSE = \frac{1}{mn} \sum_{i=0}^{m-1} \sum_{j=0}^{n-1} \|I(i,j) - K(i,j)^2 \tag{6}$$

The Peak Signal-to-Noise Ratio is defined as follows:

$$PSNR = 10 \log_{10}(\frac{MAX_I^2}{MSE}) = 20 \log_{10}(\frac{MAX_I)}{\sqrt{MSE}} \tag{7}$$

where "MAX" represents the maximum color value for image pixels. If each sampling point is represented using 8 bits, it would be 255.

The Gray Mean Gradient (GMG), employed to reflect image contrast, detail variations, and texture characteristics, is commonly utilized to assess image blurriness. A higher GMG value indicates richer image details, clearer textures, and better image quality. The GMG function is defined as follows:

$$GMG = \frac{1}{(M-1) \times (N-1)} \sum_{i-1}^{M-1} \sum_{j=1}^{N-1} \sqrt{\frac{[g(i,j+1) - g(i,j)]^2 + [g(i+1,j) - g(i,j)]^2}{2}} \tag{8}$$

The information entropy H reflects the grayscale information of pixel positions in an image and the comprehensive characteristics of grayscale distribution within pixel neighborhoods. It serves as a measure of the information content in an image. A higher entropy value indicates a greater amount of information. The formula for its definition is as follows:

$$H = -\sum_{r=0}^{L-1} \frac{H_r}{M \times N \times D} \log \frac{H_r}{M \times N \times D} \tag{9}$$

where L stands for the maximum grayscale level of the image; H_r represents the count of pixels with a grayscale value of r in the image; M, N, and D respectively denote the length, width, and dimension of the image.

In addition, this section will also compare the algorithm proposed in this study with the contrast enhancement evaluation method introduced by Hautiere, a French scholar [13]. Based on the contrast enhancement evaluation method rooted in visible edges [13], the approach primarily relies on the International Commission on Illumination's atmospheric visibility definition. It combines this definition with the Logarithmic Image Processing (LIP) model to derive contrast maps. By utilizing three metrics: the ratio of newly visible edges after complex enhancement (e), the normalized gradient mean of visible variations ($\overline{r}$), and the percentage of saturated black or white pixels (σ), this methodology objectively assesses the dehazing efficacy of different algorithms from distinct perspectives.

TABLE 1. Perormance comparison on synthetic datasets.

Database	Metrics	IQA methods							
		PSNR	SSIM	AG	Entropy	e	$\overline{r}$	σ	Ours
Aerial	SROCC	0.765	0.632	0.541	0.504	0.368	0.331	0.357	0.865
	PLCC	0.721	0.612	0.532	0.501	0.378	0.312	0.337	0.843
	RMSE	5.786	6.351	9.886	9.754	10.785	11.968	11.968	5.234
Building	SROCC	0.756	0.674	0.532	0.534	0.401	0.387	0.331	0.841
	PLCC	0.771	0.645	0.521	0.512	0.398	0.346	0.321	0.867
	RMSE	5.754	6.341	9.876	9.653	11.986	11.964	8.696	5.674
Forest	SROCC	0.765	0.681	0.541	0.541	0.398	0.365	0.331	0.867
	PLCC	0.750	0.674	0.523	0.523	0.378	0.321	0.312	0.851
	RMSE	5.872	6.423	9.535	9.985	11.795	12.886	8.864	5.321
City	SROCC	0.734	0.691	0.551	0.519	0.410	0.332	0.314	0.810
	PLCC	0.744	0.687	0.545	0.501	0.397	0.312	0.301	0.828
	RMSE	5.684	6.351	9.944	9.865	12.912	12.853	8.124	5.012
Indoor	SROCC	0.731	0.676	0.512	0.488	0.386	0.299	0.286	0.799
	PLCC	0.743	0.634	0.514	0.487	0.365	0.297	0.287	0.831
	RMSE	5.464	6.254	9.786	9.785	12.995	12.975	12.234	5.045
Beach	SROCC	0.734	0.654	0.504	0.478	0.399	0.278	0.289	0.676
	PLCC	0.725	0.645	0.501	0.456	0.383	0.297	0.275	0.664
	RMSE	5.842	6.101	8.899	9.421	11.986	12.786	12.542	5.775

$$e = \frac{n_r - n_0}{n_0} \tag{10}$$

$$\overline{r} = \exp[\frac{1}{n_r} \sum_{P_i \in \Psi_r} \log r_i] \tag{11}$$

$$\sigma = \frac{n_s}{\dim_x \times \dim_y} \tag{12}$$

where e signifies the proportion of newly visible edges, which can be determined by calculating the number of visible edges before enhancement (n_0) and after enhancement (n_r) using the Canny edge detection method; $\overline{r}$ denotes the normalized mean gradient of edges. The set of all visible edges in the processed image is represented as Ψ_r, P_i stands for pixels positioned on the edge, and r_i is the gradient ratio of individual pixels on the edge (gradients are typically computed using the Sobel operator); σ stands for the ratio of saturated black or white pixels. n_s represents the count of such pixels in the image. $\dim_x$ and $\dim_y$ are the pixel width and height of the image under evaluation.

For each algorithm, the ideal dehazing effect should inherently maintain appropriate image contrast without sacrificing visual information. In the context of the contrast enhancement evaluation based on visible edges, higher values of e and $\overline{r}$ and lower values of σ indicate better dehazing results.

4.2. **Comparison on image quality assessment.** As can be seen from Table 1, the method proposed in this paper outperforms the state-of-the-art IQA algorithm in the vast majority of cases. These include referenced PSNR and SSIM, possibly because they have difficulty learning perceptual rules or meta-knowledge about image dehazing. In addition to this, the results show taht classical IQA algorithms such as AG and Entropy different significantly from the dehazing quality evaluation algorithms.

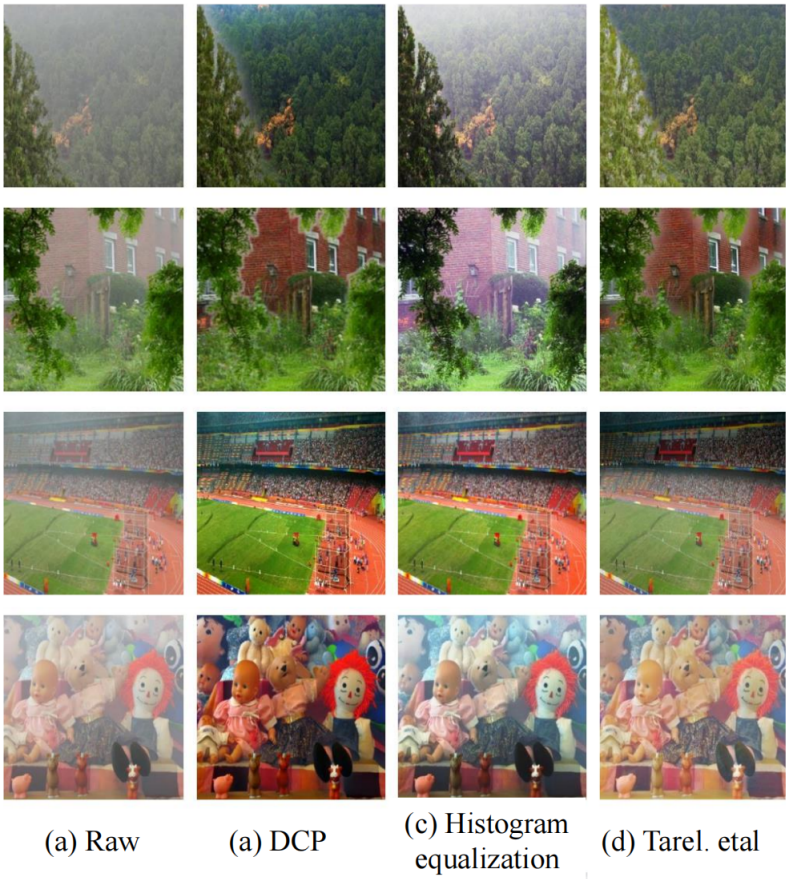

FIGURE 5. Comparison of dehazing performance among different algorithms.

To validate the performance of the proposed algorithm, a comparison was conducted with the methods introduced in references [6], histogram equalization, and the approach proposed in reference [28]. The dehazing effects are illustrated in Figure 5, and the experimental results are presented in Tables 2.

From Figure 5, it is evident that although image (c) exhibits enhanced details in the foreground, yielding a slightly improved effect, the overall dehazing performance is comparatively poorer in most areas, resulting in an inferior visual outcome compared to the dehazing effects of (b) and (d). Upon observing images (b) and (d), it's apparent that image (d) retains a smaller amount of residual haze in regions with abrupt depth changes and maintains a thin layer of haze in other areas. Consequently, the dehazing effect of (d) is not as effective as that of (b). Therefore, based on visual observation, the dehazing effect of (b) is better than that of (d), and (d) is better than (c). Continuing to examine images (f), (g), and (h), it can be seen that although image (g) has a slightly better effect in the foreground, the dehazing performance is poorer in most regions, resulting in an inferior overall visual outcome compared to (f) and (h). Further observation of images (f) and (h) reveals that both exhibit residual haze in areas with abrupt depth changes, with image (f) retaining a small amount of haze, while image (h) contains a considerable amount of residual haze. Hence, the dehazing effect of (h) is not as good as that of (f). Therefore, based on visual observation, the dehazing effect of (j) is better than (k), and (j) is better than (l). Continuing to observe images (n), (o), and (p), it's apparent that image (n) features vibrant colors and significantly better contrast than images (o) and (p). Further observation of images (o) and (p) reveals that although image (p) has slightly higher contrast compared to image (o), they both exhibit a visually similar thin

layer of haze. However, the bottom dehazing effect of image (o) is noticeably superior to that of image (p). Therefore, based on visual observation, the dehazing effect of image (n) is better than that of (o), and (o) is better than (p). Continuing to examine images (j), (k), and (l), the overall performance of image (l) is notably inferior to (j) and (k). Hence, based on visual observation, the dehazing effect of (k) is better than (l), and (l) is better than (j). Continuing to observe images (j) and (k), both exhibit similar overall characteristics, but image (j) displays a noticeably better dehazing effect in the audience area compared to the corresponding portion of image (k).

TABLE 2. Objective evaluation of Figure 5 by three image quality evaluation algorithms.

Images	PSNR	AG	Entropy
(b)	10.7535	4.6197	16.5300
(c)	14.6951	4.8458	13.2733
(d)	13.8248	7.3011	15.8010
(f)	12.2096	6.9587	15.8977
(g)	10.7010	7.2212	14.3344
(h)	12.4057	5.8980	16.6127
(j)	10.0334	11.1157	16.0541
(k)	11.2783	9.2780	16.0923
(l)	10.9687	7.5816	15.7942
(n)	10.7883	3.4181	16.3161
(o)	13.2242	2.7080	14.0193
(p)	13.2823	3.1054	15.6599

From Table 2, we can observe that the evaluation based on Peak Signal-to-Noise Ratio (PSNR) suggests that the effect of image (c) is better than (d) and (b), the effect of image (k) is superior to (j), and the effect of image (n) is inferior to both (o) and (p). The evaluation based on Mean Gradient indicates that the effect of (g) is better than (f). Moreover, the evaluation derived from Information Entropy implies that the effect of image (h) is superior to (f). These data results are inconsistent with our observations.

Hence, from Table. 2, we can infer that traditional image evaluation algorithms are inadequate for assessing dehazing quality.

TABLE 3. Literature [13] computed for each of the dehazing image evaluation metrics.

metric	(b)	(c)	(d)	(e)	(f)	(g)
e	1.7348	0.8237	1.4449	0.21386	0.095142	0.19748
$\overline{r}$	2.6142	2.2477	3.4905	2.1801	1.7653	1.6039
σ	0.0547%	0.0019%	0.0270%	4.1827%	0.0003%	3.7578%
metric	(h)	(i)	(j)	(k)	(l)	(m)
e	0.6015	0.4761	0.4605	2.2009	1.2912	0.6397
$\overline{r}$	3.3404	3.0051	2.5417	3.5538	2.6084	3.793
σ	2.7761%	2.4141%	0.0050%	1.8468%	0.0002%	0.0012%

Reference [13] indicates that an ideal dehazing effect should necessarily have proper image contrast without losing visual information. In the visible edge-based contrast enhancement evaluation method, the larger the e and $\overline{r}$, the smaller the value of σ, indicating

the better the dehazing effect [13]. Table. 3 shows the results of the calculation of each dehazing image in Figure 5 using the above three indicators. It is noted that the value may be negative, mainly because for some dehazed images, although the number of visible pixels has increased significantly compared to the original image, the number of visible edges of the dehazed image consisting of these visible pixels is reduced compared to that of the original image when counting these visible pixels, resulting in a negative value.

When using the contrast enhancement evaluation method to quantitatively evaluate the dehazing effect, it should be ensured that the same evaluation result can be obtained by using any of the indexes in the method, i.e., the better dehazing algorithm should satisfy the larger e and $\overline{r}$, as well as the smaller σ value at the same time, but it can be seen that this is not the case for the evaluation results from Table 3.

TABLE 4. The algorithm proposed in this paper compares the objective evaluation metrics of Figure 7.

Original	[6]	Histogram Equalization	[28]
(a)	28.3243	14.6347	20.2835
(e)	19.5247	11.7686	16.6035
(i)	26.7615	18.7928	17.6118
(m)	36.0446	12.9137	11.9877

Upon examining the data presented in Tables 2 and 3, it becomes evident that the utilization of peak signal-to-noise ratio, mean gradient, information entropy, and contrast enhancement assessment based on visible edges, as outlined in the work of reference [13], all fall short in precisely evaluating the efficacy of image dehazing.

From Table 4, it can be discerned that the evaluation of image dehazing effects generated by the algorithm proposed in this study aligns with the outcomes derived from our human visual perception. This congruence substantially substantiates the precision of the algorithm presented in this paper.

As illustrated in Figure 6, seven distinct regions imbued with haze have been demarcated utilizing rectangular boxes of varying colors and dimensions, each measuring 15 by 15 units. Subsequently, we proceed to appraise these eight delineated regions employing the algorithm introduced within this paper.

The coordinates of the centers of the red, orange, yellow, green, blue, white, black, and purple boxes are (106,15), (212,104), (183,182), (167,258), (487,13), (480,51), (606,279), and (232,49), respectively.

TABLE 5. Pixels with notable dehazing efficacy in Figure 6 along with their corresponding scores.

(106,15)	(212,104)	(183,182)	(167,258)
5.7603	9.1209	6.6716	10.3665
(487,13)	(460,51)	(636,279)	(232,49)
7.4423	8.9771	9.9261	8.2583

From Table 5, it is evident that for the eight subregions with subpar dehazing effects identified through visual inspection, the algorithm proposed in this study assigns significantly lower scores to each individual subregion as compared to the score attributed to the entire image. This disparity underscores the algorithm's capability to discern regions where the dehazing effect is notably inferior to the average effect across the entire image.

FIGURE 6. The evaluation scores for the above eight 15*15 regions are shown in table 5.

This observation further underscores the utility of the proposed evaluation algorithm not only for assessing entire images but also for precise evaluation at the level of individual pixels.

5. **Conclusion.** In contrastive experiments, the proposed dehazed image evaluation methodology is compared against three commonly employed image assessment metrics: Peak Signal-to-Noise Ratio (PSNR), Mean Gradient, and Information Entropy, alongside an algorithm designed specifically for evaluating dehazing effects. Experimental findings underscore that the dehazed image evaluation approach put forth in this study not only offers comprehensive image assessment capabilities but also exhibits precision in evaluating specific regions. The outcomes of this evaluation are characterized by objectivity and fairness, and they notably align with subjective human visual judgments. Moreover, the proposed methodology proves versatile in its capacity to assess a diverse array of dehazing algorithms.

Acknowledgment. This work was jointly supported by the Young and Middle-aged Teacher Education Research Project of Fujian Province (Science and Technology, Project No. JAT220829, and JAT210410), the project of Digital Media Art, Key Laboratory of Sichuan Province (Sichuan Conservatory of Music, Project No. 21DMAKL01), the first batch of industry-university cooperation collaborative education project funded by the Ministry of Education of the People's Republic of China (Minjiang University, Project No. 202101071001), Minjiang University 2021 school-level scientific research project (Minjiang University, Project No. MYK21011), Open Fund Project of Fuzhou Technology Innovation Center of Intelligent Manufacturing Information System (Minjiang University, Grant No. MJUKF-FTICIMIS2022), Open Fund Project of Engineering Research Center for ICH Digitalization and Multi-source Information Fusion (Fujian Polytechnic Normal University, Grant No. G3-KF2204), Guiding Project of Fujian Province (Minjiang University, Project No. 2020H0046). Key Technology Research and Industrialization Project for

Software Industry Innovation in Fujian Province (MinjiangUniversity and Fujian Guotong Information Technology Co., Ltd., Project No. 36).

REFERENCES

[1] C. Wang, Z. Li, J. Wu, H. Fan, G. Xiao, and H. Zhang, "Deep residual haze network for image dehazing and deraining," *IEEE Access*, vol. 8, pp. 9488–9500, 2020.

[2] C. Wang, A. Grau, E. Guerra, Z. Shen, J. Hu, and H. Fan, "Semi-supervised wildfire smoke detection based on smoke-aware consistency," *Frontiers in Plant Science*, vol. 13, p. 980425, 11 2022.

[3] F. Zhang, T.-Y. Wu, J.-S. Pan, G. Ding, and Z. Li, "Human motion recognition based on svm in vr art media interaction environment," *Human-centric Computing and Information Sciences*, vol. 9, pp. 1–15, 2019.

[4] F. Zhang, T.-Y. Wu, and G. Zheng, "Video salient region detection model based on wavelet transform and feature comparison," *EURASIP Journal on Image and Video Processing*, vol. 2019, no. 1, pp. 1–10, 2019.

[5] R. Fattal, "Single image dehazing," *Acm Transactions on Graphics*, vol. 27, no. 3, pp. 1–9, 2008.

[6] K. He, J. Sun, and X. Tang, "Single image haze removal using dark channel prior," *IEEE Transactions on Pattern Analysis and Machine Intelligence*, vol. 33, no. 12, pp. 2341–2353, 2010.

[7] Z. Wang, "Image quality assessment : From error visibility to structural similarity," *IEEE Transactions on Image Processing*, vol. 13, no. 4, pp. 600–612, 2004.

[8] W. Zhou and A. C. Bovik, "A universal image quality index," *IEEE Signal Processing Letters*, vol. 9, no. 3, pp. 81–84, 2002.

[9] W. Zhou, A. C. Bovik, and L. Lu, "Why is image quality assessment so difficult?," *IEEE International Conference on Acoustics*, pp. 3313–3316, 2002.

[10] M. Tao, X. S. Hua, C. Z. Zhu, H. Q. Zhou, and S. Li, "Home video visual quality assessment with spatiotemporal factors," *IEEE Transactions on Circuits & Systems for Video Technology*, vol. 17, no. 6, pp. 699–706, 2007.

[11] M. Carnec, P. L. Callet, and D. Barba, "Objective quality assessment of color images based on a generic perceptual reduced reference," *Signal Processing Image Communication*, vol. 23, no. 4, pp. 239–256, 2008.

[12] H. R. Sheikh, A. C. Bovik, and L. Cormack, "No-reference quality assessment using natural scene statistics: Jpeg2000," *IEEE Transactions on Image Processing*, vol. 14, no. 11, pp. 1918–1927, 2005.

[13] N. Hautiere, J. P. Tarel, D. Aubert, and E. Dumont, "Blind contrast enhancement assessment by gradient ratioing at visible edges," *Image Analysis & Stereology*, vol. 27, no. 2, pp. 87–95, 2011.

[14] D. Li, J. Yu, C. Xiao, *et al.*, "No-reference quality assessment method for defogged images," *Journal of Image and Graphics*, vol. 16, no. 9, pp. 1753–1757, 2011.

[15] A. K. Moorthy and A. C. Bovik, "Blind image quality assessment: From natural scene statistics to perceptual quality," *IEEE Transactions on Image Processing*, vol. 20, no. 12, pp. 3350–3364, 2011.

[16] M. A. Saad, A. C. Bovik, and C. Charrier, "Blind image quality assessment: A natural scene statistics approach in the dct domain," *IEEE Transactions on Image Processing*, vol. 21, no. 8, pp. 3339–3352, 2012.

[17] K. He, X. Zhang, S. Ren, and J. Sun, "Deep residual learning for image recognition," in *Proceedings of the IEEE Conference on Computer Vision and Pattern Recognition*, pp. 770–778, 2016.

[18] O. Russakovsky, J. Deng, H. Su, J. Krause, S. Satheesh, S. Ma, Z. Huang, A. Karpathy, A. Khosla, M. Bernstein, *et al.*, "Imagenet large scale visual recognition challenge," *International Journal of Computer Vision*, vol. 115, pp. 211–252, 2015.

[19] W. Zhang, K. Ma, J. Yan, D. Deng, and Z. Wang, "Blind image quality assessment using a deep bilinear convolutional neural network," *IEEE Transactions on Circuits and Systems for Video Technology*, vol. 30, no. 1, pp. 36–47, 2018.

[20] J. Kim and S. Lee, "Fully deep blind image quality predictor," *IEEE Journal of Selected Topics in Signal Processing*, vol. 11, no. 1, pp. 206–220, 2016.

[21] H. Zeng, L. Zhang, and A. C. Bovik, "A probabilistic quality representation approach to deep blind image quality prediction," *arXiv preprint arXiv:1708.08190*, 2017.

[22] S. Su, Q. Yan, Y. Zhu, C. Zhang, X. Ge, J. Sun, and Y. Zhang, "Blindly assess image quality in the wild guided by a self-adaptive hyper network," in *Proceedings of the IEEE/CVF Conference on Computer Vision and Pattern Recognition*, pp. 3667–3676, 2020.

[23] Z. Ying, H. Niu, P. Gupta, D. Mahajan, D. Ghadiyaram, and A. Bovik, "From patches to pictures (paq-2-piq): Mapping the perceptual space of picture quality," in *Proceedings of the IEEE/CVF Conference on Computer Vision and Pattern Recognition*, pp. 3575–3585, 2020.

[24] S. G. Narasimhan and S. K. Nayar, "Vision and the atmosphere," *International Journal of Computer Vision*, vol. 48, no. 3, pp. 233–254, 2002.

[25] J. Kopf, B. Neubert, B. Chen, M. Cohen, D. Cohen-Or, O. Deussen, M. Uyttendaele, and D. Lischinski, "Deep photo: model-based photograph enhancement and viewing," *Acm Transactions on Graphics*, vol. 27, no. 5, pp. 1–10, 2008.

[26] E. K. Wang, X. Zhang, F. Wang, T.-Y. Wu, and C.-M. Chen, "Multilayer dense attention model for image caption," *IEEE Access*, vol. 7, pp. 66358–66368, 2019.

[27] T.-Y. Wu, X. Fan, K.-H. Wang, J.-S. Pan, and C.-M. Chen, "Security analysis and improvement on an image encryption algorithm using chebyshev generator," *Journal of Internet Technology*, vol. 20, no. 1, pp. 13–23, 2019.

[28] J. P. Tarel and N. Hautière, "Fast visibility restoration from a single color or gray level image," *IEEE International Conference on Computer Vision*, vol. 30, no. 2, pp. 2201–2208, 2010.